

The Inverse Problem of Determining Heat Transfer Coefficients by the Meshless Local Petrov-Galerkin Method

J. Sladek¹, V. Sladek¹, P.H. Wen² and Y.C. Hon³

Abstract: The meshless local Petrov-Galerkin (MLPG) method is used to solve the inverse heat conduction problem of predicting the distribution of the heat transfer coefficient on the boundary of 2-D and axisymmetric bodies. Using this method, nodes are randomly distributed over the numerical solution domain, and surrounding each of these nodes, a circular sub-domain is introduced. By choosing a unit step function as the test function, the local integral equations (LIE) on the boundaries of these sub-domains are derived. To eliminate the time variation in the governing equation, the Laplace transform technique is applied. The local integral equations are nonsingular and take a very simple form. The spatial variations of the Laplace transforms of temperature and heat flux are approximated on the local boundary and in the interior of the subdomain by means of the moving least-squares (MLS) method. The truncated singular value decomposition (TSVD) is applied to solve the ill-conditioned linear system of algebraic equations obtained from the LIE after the MLS approximation. The Stehfest algorithm is then applied for the numerical Laplace inversion, in order to retrieve the time-dependent solutions. The effectiveness of the MLPG method for this inverse problem is demonstrated by some numerical examples.

Keywords: Transient inverse heat conduction problem, Laplace transform, Stehfest algorithm, Singular value decomposition, Meshless approximation; Moving-least-squares method.

¹ Institute of Construction and Architecture, Slovak Academy of Sciences, 84503 Bratislava, Slovakia, e-mail: sladek@savba.sk

² Department of Civil Engineering, Queen Mary University of London, Mile End, London E14NS, U.K.

³ Department of Mathematics, City University of Hong Kong, Hong Kong

1 Introduction

The heat transfer coefficient is a very important parameter in the analysis of heat transfer problems. It is usually determined empirically from direct correlations of experimental data. The success of these experiments is, however, often limited to some range of flow parameters and to steady state conditions. As a result, many investigators have developed various inverse schemes for determining this quantity [Osman and Beck (1990), Kurpisz and Nowak (1995), Martin and Dulikravich (1998), Duda and Taler (2000), Chantasiriwan (2000), Ling et al. (2003), Chen and Wu (2006), Chen and Chou (2006)]. To solve the inverse heat conduction problem (IHCP), only the temperatures at some interior points need to be measured; they are usually on the symmetric axes, if any, where there is vanishing heat flux. The unknown temperature and heat flux at the exterior boundary are computed utilizing the measured temperatures and prescribed heat fluxes on the remaining part of the boundary of the analyzed domain. By solving this problem instead, the errors introduced by the boundary or interior measurements are reduced due to the diffusive character of the heat conduction process. However, it is well known that inverse problems are, in general, unstable [Hadamard (1923), Ling and Atluri (2006)] in the sense that small measurement errors in the input data may amplify significantly the errors in the solution. Many of the traditional computational methods for well-posed direct problems fail to produce acceptable solutions to such inverse problems. Several techniques have been proposed for solving a one-dimensional IHCP [Beck et al. (1985), Chantasiriwan (1989), Lesnic et al. (1996), Lesnic and Elliot (1999), Jonas and Louis (2000), Shen (1999), Hon and Wei (2004)]. The methods which have been widely adopted for treating two-dimensional IHCP's include the boundary element [Chantasiriwan (2001), Kurpisz and Nowak (1992), Mera et al. (2000)], finite difference [Guo and Murio (1991), Khalidy (1998)] and finite elements [Hsu et al. (1992), Reinhardt (1991)] methods, the group preserving scheme [Chang et al. (2005), Liu (2006)], as well as the Trefftz method [Liu (2008)] and the method of fundamental solutions [Hon and Wei (2005)]. There remains a need for developing efficient and versatile numerical schemes for analysing the multi-dimensional IHCP. Recently, Liu et al. (2009a) have introduced a novel and general approach to resolve the ill-posedness of highly ill-conditioned system of linear equations by utilizing a discrete solution of the PDE of the Laplacian type. Pre/post conditioner is obtained for the Laplace equation through a boundary-collocation Trefftz method. Quality of the conditioner is greatly enhanced by using multipole characteristic lengths in the Trefftz expansion. A novel interpolation technique [Liu and Atluri (2009b)] has been developed also to solve accurately some ill-posed linear problems, such as the numerical differentiation of noisy data and computation of the inverse Laplace transform. Also Liu

and Atluri (2009c) have applied the fictitious time integration method (FTIM) to solve a system of ill-posed linear equations. The fictitious time plays there the role of a regularization parameter, and its filtering effect is better than that of the Tikhonov and the exponential filters.

In spite of the great success of the finite and boundary element methods as effective numerical tools for the solution of boundary value problems on complex domains, their shortcomings have spurred a growing interest in the development of new advanced computational methods. Meshless methods have emerged as a competitive alternative to these classical discretization techniques due to their high adaptability and the low cost in the preparation of input data for numerical analyses. Several such methods have been proposed in the literature, see, e.g., [Belytschko et al. (1996), Atluri (2004), Atluri and Zhu (1998), Sladek et al. (2006), Li et al. (2002), Kansa (1990), Golberg and Chen (1998), Chen and Tanaka (2002)]. A more recent and novel approach based on the local Petrov-Galerkin method [Atluri and Shen (2002), Atluri et al. (2003)] has also been proposed for various boundary value problems and to solve the heat conduction problems too [Sladek et al. (2004) (2003a,b) (2005a,b)]. The analyzed domain can be divided into small sub-domains with simple geometry. For each of these sub-domains, the fundamental solutions of some simplified differential operators or a parametrix (Levi function) [Mikhailov (2002)] can then be found. On the surface of each sub-domain, the local integral equations (LIE) are expressed in the Laplace transform domain to eliminate the time dependence variable of the governing equation for transient heat conduction problems. The idea has been successfully applied to 2-D transient heat conduction analysis [Sladek et al. (2004) (2003a,b) (2005a,b)]. The authors have further applied the approach to analyze transient heat conduction problems in axisymmetric and isotropic functionally graded materials (FGM's) [Sladek et al. (2003b)]. Recently, Sladek et al. [Sladek et al. (2003a,b) (2005a,b)] have also proposed a meshless method based on the local Petrov-Galerkin approach to solve stationary and transient heat conduction problems in 2-D anisotropic FGM's and for 3-D problems [Sladek et al. (2008)]. The anisotropy increases the number of heat conduction constants, which renders the derivation of fundamental solutions very difficult to obtain even in a homogeneous case.

In this paper, the meshless local Petrov-Galerkin (MLPG) method is used to solve transient inverse heat conduction problems in 2-D and axisymmetric bodies. For the latter, axial symmetry of the geometry and boundary conditions reduces the original 3-D boundary value problem to a 2-D problem about the radial plane. In the MLPG approach here, nodes may be randomly scattered over the numerical solution domain. Surrounding each of these nodes, a small circular sub-domain is introduced. The Laplace transform technique is applied to eliminate the time vari-

able in the governing differential equation; the original linear parabolic differential equation is thereby converted into a linear elliptic one. A unit step function is chosen as the test function to derive the local integral equations on the boundaries of the sub-domains; these local integral equations (LIE's) have a boundary-domain integral form. In contrast to the global formulation based on boundary-domain integral equations, the present boundary-domain integral formulation on local sub-domains is much easier for numerical computations as the LIE's are nonsingular and they take a very simple form. The spatial variations of the Laplace transforms of the temperature and heat flux on the sub-domain are approximated by the moving least-squares (MLS) method. To solve the ill-conditioned linear system of algebraic equations obtained from the LIE's after MLS approximation [Shenefelt et al. (2002)], the truncated singular value decomposition is applied. The L-curve method is used to determine the regularization parameter; the regularization is especially important for "noisy" input data [Lesnic et al. (1998), Jin and Marin (2007), Divo et al. (2005)]. Several quasi-static boundary value problems are solved for various values of the Laplace transform parameter. The Stehfest [Stehfest (1970)] numerical inversion scheme is employed to obtain the time-dependent solutions. Numerical examples involving a finite strip and a hollow cylinder with orthotropic and functionally graded material properties are analyzed to verify the efficiency and accuracy of the proposed computational method.

2 Local integral equations for 2-D problems

Consider a finite 2-D body, with initial temperature T , in a moving fluid which has temperature $\theta_e(t)$. The solid body, in the general case, has continuously varying anisotropic material properties, and the unknown heat transfer coefficients on parts of the boundary are to be determined. The boundary value problem for the heat conduction in the body is governed by the following equation:

$$\rho(\mathbf{x})c(\mathbf{x})\frac{\partial\theta}{\partial t}(\mathbf{x},t)=[k_{ij}(x)\theta_{,j}(\mathbf{x},t)]_{,i}+Q(\mathbf{x},t), \quad (1)$$

where $\theta(\mathbf{x},t)$ is the temperature field, $Q(\mathbf{x},t)$ is the density of body heat source, k_{ij} is the thermal conductivity tensor, $\rho(\mathbf{x})$ is the mass density and $c(\mathbf{x})$ the specific heat.

In the present analysis, only numerical experiments are used to provide the temperatures at internal points which are selected on symmetric axes. Thus, no other internal node temperatures are prescribed in the inverse problems treated in this study. The global boundary Γ consists of three parts $\Gamma = \Gamma_\theta \cup \Gamma_q \cup \Gamma_3$ and the following boundary and initial conditions are assumed

$$\theta(\mathbf{x},t) = \tilde{\theta}(\mathbf{x},t) \text{ on } \Gamma_\theta$$

$$\begin{aligned}
 q(\mathbf{x}, t) &= k_{ij}(\mathbf{x})\theta_{,j}(\mathbf{x}, t)n_i(\mathbf{x}) = \tilde{q}(\mathbf{x}, t) \text{ on } \Gamma_q \\
 q(\mathbf{x}, t) &= h(\mathbf{x})[\theta_e(t) - \theta(\mathbf{x}, t)] \text{ on } \Gamma_3 \\
 \theta(\mathbf{x}, t)|_{t=0} &= T(\mathbf{x}, 0),
 \end{aligned} \tag{2}$$

where n_i is the unit outward normal at the global boundary; $h(\mathbf{x})$ is unknown heat transfer coefficient; $\theta_e(t)$ is the temperature of the fluid medium outside of solid body; Γ_θ is the part of the global boundary with prescribed temperature; on Γ_q , the heat flux is prescribed; and, Γ_3 represents the part of the surface where convective boundary condition is prescribed. Generally, the heat transfer coefficient on some part of the surface can be prescribed and on some part, it is unknown $\Gamma_3^* \subset \Gamma_3$. The main goal of this paper is to determine the unknown heat transfer coefficient from the Dirichlet and Neumann data prescribed on the accessible part of the boundary $\Gamma_1 \subset \Gamma$, i.e.

$$\theta(\mathbf{x}, t) = \tilde{\theta}(\mathbf{x}, t), \quad \mathbf{x} \in \Gamma_1, \quad t \in (0, t_{\max})$$

$$q(\mathbf{x}, t) = \tilde{q}(\mathbf{x}, t), \quad \mathbf{x} \in \Gamma_1, \quad t \in (0, t_{\max}).$$

For uniqueness of the solution, only examples where temperature and heat flux are defined simultaneously on some part of the boundary are considered here. Once the temperature and heat flux are computed everywhere, the unknown heat transfer coefficient can be easily obtained from the third equation in equation (2).

Applying the Laplace transformation

$$L[\theta(\mathbf{x}, t)] = \bar{\theta}(\mathbf{x}, s) = \int_0^\infty \theta(\mathbf{x}, t)e^{-st} dt,$$

to the governing equation (1) results in the following

$$[k_{ij}(\mathbf{x})\bar{\theta}_{,j}(\mathbf{x}, s)]_{,i} - \rho(\mathbf{x})c(\mathbf{x})s\bar{\theta}(\mathbf{x}, s) = -\bar{F}(\mathbf{x}, s), \tag{3}$$

where

$$\bar{F}(\mathbf{x}, s) = \bar{Q}(\mathbf{x}, s) + \theta(\mathbf{x}, 0)$$

is the redefined body heat source in the Laplace transform domain with initial boundary condition for temperature, and s is the Laplace transform parameter.

Instead of working with the global weak form for the above governing equation, the MLPG methods construct the weak form over local sub-domains, such as Ω_s ,

which is a small region taken around each node inside the global domain [Sladek et al. (2006)]. The local sub-domains overlap each other, and cover the whole global domain Ω ; they could be of any geometric shape and size. In the present work, these local sub-domains are taken to be of circular shape. The local weak form of the governing equation (3) for $\mathbf{x}^a \in \Omega_s^a$ can be written as

$$\int_{\Omega_s^a} \left[(k_{ij}(\mathbf{x})\bar{\theta}_{,j}(\mathbf{x},s))_{,i} - \rho(\mathbf{x})c(\mathbf{x})s\bar{\theta}(\mathbf{x},s) + \bar{F}(\mathbf{x},s) \right] \theta^*(\mathbf{x}) d\Omega = 0, \tag{4}$$

where $\theta^*(\mathbf{x})$ is a weight (test) function. Using

$$(k_{ij}(\mathbf{x})\bar{\theta}_{,j}(\mathbf{x},s))_{,i} \theta^*(\mathbf{x}) = (k_{ij}(\mathbf{x})\bar{\theta}_{,j}(\mathbf{x},s)\theta^*(\mathbf{x}))_{,i} - k_{ij}(\mathbf{x})\bar{\theta}_{,j}(\mathbf{x},s)\theta^*_{,i}(\mathbf{x})$$

and applying the Gauss divergence theorem one can write

$$\begin{aligned} & \int_{\partial\Omega_s^a} \bar{q}(\mathbf{x},s)\theta^*(\mathbf{x})d\Gamma - \int_{\Omega_s^a} k_{ij}(\mathbf{x})\bar{\theta}_{,j}(\mathbf{x},s)\theta^*_{,i}(\mathbf{x})d\Omega - \int_{\Omega_s^a} \rho(\mathbf{x})c(\mathbf{x})s\bar{\theta}(\mathbf{x},s)\theta^*(\mathbf{x})d\Omega + \\ & + \int_{\Omega_s^a} \bar{F}(\mathbf{x},s)\theta^*(\mathbf{x})d\Omega = 0, \end{aligned} \tag{5}$$

where $\partial\Omega_s^a$ is the boundary of the local sub-domain and

$$\bar{q}(\mathbf{x},s) = k_{ij}(\mathbf{x})\bar{\theta}_{,j}(\mathbf{x},s)n_i(\mathbf{x}).$$

The local weak form, equation (5), is a starting point for the derivation of the local boundary integral equations. An appropriate test function needs to be selected. To this end, a Heaviside step function may be chosen as the test function $\theta^*(\mathbf{x})$ in each sub-domain, i.e.

$$\theta^*(\mathbf{x}) = \begin{cases} 1 & \text{at } \mathbf{x} \in \Omega_s^a \\ 0 & \text{at } \mathbf{x} \notin \Omega_s^a \end{cases}$$

Equation (5) can then be transformed into the following simple local boundary integral equation

$$\int_{\partial\Omega_s^a} \bar{q}(\mathbf{x},s)d\Gamma - \int_{\Omega_s^a} \rho(\mathbf{x})c(\mathbf{x})s\bar{\theta}(\mathbf{x},s)d\Omega = - \int_{\Omega_s^a} \bar{F}(\mathbf{x},s)d\Omega. \tag{6}$$

Equation (6) is recognized as the flow balance condition of the sub-domain. Under steady-state conditions, the domain integral on the left hand side of this equation disappears. Furthermore, if body heat source is absent in the problem, a pure contour integral formulation is obtained.

3 Local boundary integral equations for axisymmetric problems

For an axisymmetric problem, it is convenient to use cylindrical polar coordinates $\mathbf{x} \equiv (r, \varphi, z)$ (Fig.1). In this case, the governing equation (1) can be rewritten in the form

$$[k_{\alpha\beta}(\mathbf{x})\theta_{,\beta}(\mathbf{x},t)]_{,\alpha} + \frac{k_{rz}(\mathbf{x})}{r}\theta_{,z}(\mathbf{x},t) + \frac{k_{rr}(\mathbf{x})}{r}\theta_{,r}(\mathbf{x},t) + Q(\mathbf{x},t) = \rho(\mathbf{x})c(\mathbf{x})\frac{\partial\theta}{\partial t}(\mathbf{x},t), \quad (7)$$

where the summation convention for repeated indices α, β , representing the coordinates r, z , is assumed.

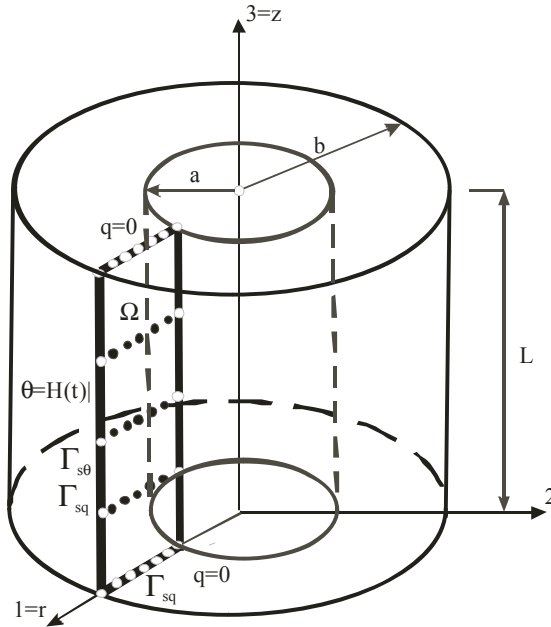


Figure 1: Boundary conditions and node distribution in analysed domain for a finite hollow cylinder

The Laplace transform when applied to equation (7) will yield

$$[k_{\alpha\beta}(\mathbf{x})\bar{\theta}_{,\beta}(\mathbf{x},s)]_{,\alpha} + \frac{k_{rz}(\mathbf{x})}{r}\bar{\theta}_{,z}(\mathbf{x},s) + \frac{k_{rr}(\mathbf{x})}{r}\bar{\theta}_{,r}(\mathbf{x},s) + \bar{F}(\mathbf{x},s) = \rho(\mathbf{x})c(\mathbf{x})s\bar{\theta}(\mathbf{x},s), \quad (8)$$

where s is the Laplace transform parameter and

$$\bar{F}(r, z, s) = \bar{Q}(r, z, s) + \theta(r, z, 0)$$

is the redefined body heat source in the Laplace transform domain with the initial boundary condition for the temperature field $\theta(r, z, 0)$. The local weak form of the governing equation (8) for $\mathbf{x}^a \in \Omega_s^a$ can be written as

$$\int_{\Omega_s^a} \left[(k_{\alpha\beta}(\mathbf{x})\bar{\theta}_{,\beta}(\mathbf{x}, s))_{,\alpha} + \frac{k_{rz}(\mathbf{x})}{r}\bar{\theta}_{,z}(\mathbf{x}, s) + \frac{k_{rr}(\mathbf{x})}{r}\bar{\theta}_{,r}(\mathbf{x}, s) - \rho(\mathbf{x})c(\mathbf{x})s\bar{\theta}(\mathbf{x}, s) + \bar{F}(\mathbf{x}, s) \right] \theta^*(\mathbf{x}) d\Omega = 0, \tag{9}$$

where $\theta^*(\mathbf{x})$ is a weight (test) function. Following the same steps as before, the Gauss divergence theorem is next applied to equation (9), which results in

$$\int_{\partial\Omega_s^a} \bar{q}(\mathbf{x}, s)\theta^*(\mathbf{x})d\Gamma - \int_{\Omega_s^a} k_{\alpha\beta}(\mathbf{x})\bar{\theta}_{,\beta}(\mathbf{x}, s)\theta^*_{,\alpha}(\mathbf{x})d\Omega - \int_{\Omega_s^a} \rho(\mathbf{x})c(\mathbf{x})s\bar{\theta}(\mathbf{x}, s)\theta^*(\mathbf{x})d\Omega + \int_{\Omega_s^a} \left[\frac{k_{rz}(\mathbf{x})}{r}\bar{\theta}_{,z}(\mathbf{x}, s) + \frac{k_{rr}(\mathbf{x})}{r}\bar{\theta}_{,r}(\mathbf{x}, s) \right] \theta^*(\mathbf{x})d\Omega + \int_{\Omega_s^a} \bar{F}(\mathbf{x}, s)\theta^*(\mathbf{x})d\Omega = 0. \tag{10}$$

If a unit step function is used as the test function $\theta^*(\mathbf{x})$ in each sub-domain, the local weak form, equation (10), is transformed into a simple local boundary integral equation

$$\int_{\partial\Omega_s^a} \bar{q}(\mathbf{x}, s)d\Gamma - \int_{\Omega_s^a} \rho(\mathbf{x})c(\mathbf{x})s\bar{\theta}(\mathbf{x}, s)d\Omega + \int_{\Omega_s^a} \left[\frac{k_{rz}(\mathbf{x})}{r}\bar{\theta}_{,z}(\mathbf{x}, s) + \frac{k_{rr}(\mathbf{x})}{r}\bar{\theta}_{,r}(\mathbf{x}, s) \right] d\Omega = - \int_{\Omega_s^a} \bar{F}(\mathbf{x}, s)d\Omega. \tag{11}$$

In the MLPG method, the test and trial functions, $\theta^*(\mathbf{x})$ and $\bar{\theta}(\mathbf{x}, s)$, are not necessarily from the same functional space. The test function is chosen as the unit step function with support on the local sub-domain. The trial function, on the other hand, is chosen to be the moving least-squares (MLS) interpolation over a number of nodes which are randomly spread within the domain of influence; this will be described in greater detail in Section 4. While the local sub-domain is defined as the support of the test function on which the integration is carried out, the domain of influence for a given node is defined as a region where the weight function is not zero. Thus, the node \mathbf{x}^a contributes to the approximation at \mathbf{x} only if this point lies at the influence domain of the node \mathbf{x}^a .

4 Meshless approximation and numerical solution

In general, a meshless method uses a local interpolation to represent the trial function with the values of the unknown variable (or the fictitious values) at some randomly located nodes. The moving least-squares (MLS) approximation [Belytschko et al. (1996), Atluri (2004)] used in the present analysis may be considered as one such scheme.

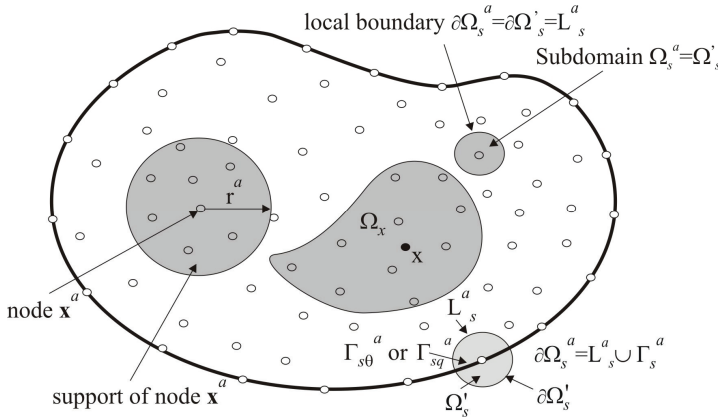


Figure 2: Local boundaries, the domain Ω_x for MLS approximation of the trial function $\theta(\mathbf{x})$, and support area of weight function around node \mathbf{x}^a

With reference to Fig. 2, consider a sub-domain Ω_x of the problem domain Ω in the neighbourhood of a point \mathbf{x} , for defining the MLS approximation of the trial function (i.e. the temperature distribution) around \mathbf{x} . To approximate the distribution of the Laplace transform of temperature in Ω_x over a number of randomly located nodes $\{\mathbf{x}^a\}$, $a = 1, 2, \dots, n$, the MLS approximant $\bar{\theta}^h(\mathbf{x}, s)$ of $\bar{\theta}$, $\forall \mathbf{x} \in \Omega_x$, is defined by

$$\bar{\theta}^h(\mathbf{x}, s) = \mathbf{p}^T(\mathbf{x})\mathbf{a}(\mathbf{x}, s), \quad \forall \mathbf{x} \in \Omega_x \tag{12}$$

where $\mathbf{p}^T(\mathbf{x}) = [p^1(\mathbf{x}), p^2(\mathbf{x}), \dots, p^m(\mathbf{x})]$ is a complete monomial basis; and $\mathbf{a}(\mathbf{x})$ is a vector containing the coefficients $a^j(\mathbf{x})$, $j = 1, 2, \dots, m$ which are functions of the space co-ordinates $\mathbf{x} = [x_1, x_2, x_3]^T$. For example, for a 2-D problem

$$\mathbf{p}^T(\mathbf{x}) = [1, x_1, x_2], \text{ for linear basis } m = 3 \tag{13}$$

$$\mathbf{p}^T(\mathbf{x}) = [1, x_1, x_2, (x_1)^2, x_1x_2, (x_2)^2], \text{ for quadratic basis } m = 6. \tag{14}$$

The coefficient vector $\mathbf{a}(\mathbf{x})$ is determined by minimizing a weighted discrete L_2 -norm defined as

$$J(\mathbf{x}) = \sum_{a=1}^n w^a(\mathbf{x}) [\mathbf{p}^T(\mathbf{x}^a)\mathbf{a}(\mathbf{x}, s) - \hat{\theta}^a(s)]^2, \tag{15}$$

where $w^a(\mathbf{x})$ is the weight function associated with the node \mathbf{x}^a , and $w^a(\mathbf{x}) > 0$. Recall that n is the number of nodes in Ω_x for which the weight function $w^a(\mathbf{x}) > 0$ and $\hat{\theta}^a(s)$ are the fictitious nodal values, but not the nodal values of the unknown trial function $\bar{\theta}^h(\mathbf{x}, s)$ in general. The stationary condition of J in equation (14) with respect to $\mathbf{a}(\mathbf{x}, s)$

$$\partial J / \partial \mathbf{a} = 0$$

leads to the following linear relation between $\mathbf{a}(\mathbf{x}, s)$ and $\hat{\theta}(s)$

$$\mathbf{A}(\mathbf{x})\mathbf{a}(\mathbf{x}, s) - \mathbf{B}(\mathbf{x})\hat{\theta}(s) = 0, \tag{16}$$

where

$$\mathbf{A}(\mathbf{x}) = \sum_{a=1}^n w^a(\mathbf{x})\mathbf{p}(\mathbf{x}^a)\mathbf{p}^T(\mathbf{x}^a),$$

$$\mathbf{B}(\mathbf{x}) = [w^1(\mathbf{x})\mathbf{p}(\mathbf{x}^1), w^2(\mathbf{x})\mathbf{p}(\mathbf{x}^2), \dots, w^n(\mathbf{x})\mathbf{p}(\mathbf{x}^n)]. \tag{17}$$

The MLS approximation is well-defined only when the matrix \mathbf{A} in equation (16) is non-singular. A necessary condition to satisfy this requirement is that at least m weight functions are non-zero (i.e. $n \geq m$) for each sample point $\mathbf{x} \in \Omega$ and that the nodes in Ω_x are not arranged in a special pattern such as on a straight line. The solution of equation (16) for $\mathbf{a}(\mathbf{x}, s)$ and a subsequent substitution into equation (12) lead to the following relation

$$\bar{\theta}^h(\mathbf{x}, s) = \Phi^T(\mathbf{x}) \cdot \hat{\theta}(s) = \sum_{a=1}^n \phi^a(\mathbf{x})\hat{\theta}^a(s), \tag{18}$$

where

$$\Phi^T(\mathbf{x}) = \mathbf{p}^T(\mathbf{x})\mathbf{A}^{-1}(\mathbf{x})\mathbf{B}(\mathbf{x}). \tag{19}$$

In equation (18), $\phi^a(\mathbf{x})$ is usually referred to as the shape function of the MLS approximation corresponding to the nodal point \mathbf{x}^a . From equations (17) and (19), it can be seen that $\phi^a(\mathbf{x}) = 0$ when $w^a(\mathbf{x}) = 0$. In practice, $w^a(\mathbf{x})$ is often chosen such that it is non-zero within the finite size support domain of the nodal point

\mathbf{x}_i . The support domain (influence domain) of the nodal point \mathbf{x}^a is usually taken to be a circle of the radius r_i centred at \mathbf{x}^a (see Fig. 2). The radius r_i is an important parameter of the MLS approximation because it determines the range of the interaction (coupling) between the degrees of freedom defined at the nodes considered. The size of the support r^a should be large enough to cover a sufficient number of nodes in the domain of definition to ensure the regularity of the matrix \mathbf{A} . The value of n is determined by the number of nodes whose influence domains involve the approximation point \mathbf{x} . The radius of the support domain for node \mathbf{x}^a is usually selected as $r^a = 4r_{loc}$, where r_{loc} is the radius of circular sub-domain.

A 4th-order spline-type weight function is employed in the present work

$$w^a(\mathbf{x}) = \begin{cases} 1 - 6\left(\frac{d^a}{r^a}\right)^2 + 8\left(\frac{d^a}{r^a}\right)^3 - 3\left(\frac{d^a}{r^a}\right)^4 & 0 \leq d^a \leq r^a \\ 0 & d^a \geq r^a \end{cases}, \quad (20)$$

where $d^a = \|\mathbf{x} - \mathbf{x}^a\|$. The C^1 -continuity of the weight function given by equation (20) is ensured over the entire domain and hence the continuity of the temperature gradients is satisfied. The partial derivatives of the MLS shape functions are obtained as [Atluri (2004)]

$$\phi_{,k}^a = \sum_{j=1}^m \left[p_{,k}^j (\mathbf{A}^{-1} \mathbf{B})^{ja} + p^j (\mathbf{A}^{-1} \mathbf{B}_{,k} + \mathbf{A}_{,k}^{-1} \mathbf{B})^{ja} \right], \quad (21)$$

wherein $\mathbf{A}_{,k}^{-1} = (\mathbf{A}^{-1})_{,k}$ represents the derivative of the inverse of \mathbf{A} with respect to x_k , which is given by

$$\mathbf{A}_{,k}^{-1} = -\mathbf{A}^{-1} \mathbf{A}_{,k} \mathbf{A}^{-1}.$$

The directional derivatives of $\bar{\theta}(\mathbf{x}, s)$ are approximated in terms of the same nodal values as $\bar{\theta}(\mathbf{x}, s)$ by

$$\frac{\partial \bar{\theta}^h}{\partial n}(\mathbf{x}, s) = n_k(\mathbf{x}) \sum_{a=1}^n \hat{\theta}^a(s) \phi_{,k}^a(\mathbf{x}). \quad (22)$$

The Laplace transform of the heat flux is then approximated by

$$\bar{q}(\mathbf{x}, s) = k_{ij}(\mathbf{x}) n_i(\mathbf{x}) \sum_{a=1}^n \hat{\theta}^a(s) \phi_{,j}^a(\mathbf{x}). \quad (23)$$

The local integral equation (6) for 2-D problems for the source point \mathbf{x}^c located

inside Ω or on Γ_3 yields the following set of equations:

$$\sum_{a=1}^n \hat{\theta}^a(s) \int_{\partial\Omega_s^c} k_{ij}(\mathbf{x}) n_j(\mathbf{x}) \phi_{,j}^a(\mathbf{x}) d\Gamma - \sum_{a=1}^n \hat{\theta}^a(s) \int_{\Omega_s^c} \rho(\mathbf{x}) c(\mathbf{x}) s \phi^a(\mathbf{x}) d\Omega = - \int_{\Omega_s^c} \bar{F}(\mathbf{x}, s) d\Omega . \quad (24)$$

The LIE at $\mathbf{x}^b \in \Gamma_{sq}^b$

$$\sum_{a=1}^n \hat{\theta}^a(s) \int_{L_s^b} k_{ij}(\mathbf{x}) n_j(\mathbf{x}) \phi_{,j}^a(\mathbf{x}) d\Gamma - \sum_{a=1}^n \hat{\theta}^a(s) \int_{\Omega_s^b} \rho(\mathbf{x}) c(\mathbf{x}) s \phi^a(\mathbf{x}) d\Omega = - \int_{\Gamma_{sq}^b} \tilde{q}(\mathbf{x}, s) d\Gamma - \int_{\Omega_s^b} \bar{F}(\mathbf{x}, s) d\Omega, \quad (25)$$

It should be noted that neither Lagrange multipliers nor penalty parameters need to be introduced into the local weak form, equation (4), since the essential boundary conditions on $\Gamma_{s\theta}^b$ can be imposed directly using the interpolation approximation of equation (18):

$$\sum_{a=1}^n \phi^a(\mathbf{x}) \hat{\theta}^a(s) = \tilde{\theta}(\mathbf{x}^b, s), \text{ for } \mathbf{x}^b \in \Gamma_{s\theta}^b \quad (26)$$

where $\tilde{\theta}(\mathbf{x}^b, s)$ is the Laplace transform of temperature prescribed on the boundary $\Gamma_{s\theta}^b$ for boundary conditions introduced below equation (2).

In a direct problem with prescribed heat transfer coefficient and thermal shock external temperature application (Heaviside time variation), the Laplace transform of heat flux on Γ_3 is given by

$$\bar{q}(\mathbf{x}, s) = h(\mathbf{x}) [\theta_{e0}/s - \bar{\theta}(\mathbf{x}, s)], \quad (27)$$

where θ_{e0} is the steady external temperature.

In such a case, the local integral equation at $\mathbf{x}^b \in \Gamma_3^b$ has the form:

$$\sum_{a=1}^n \hat{\theta}^a(s) \int_{L_s^b} k_{ij}(\mathbf{x}) n_j(\mathbf{x}) \phi_{,j}^a(\mathbf{x}) d\Gamma - \sum_{a=1}^n \hat{\theta}^a(s) \int_{\Gamma_3^b} h(\mathbf{x}) \phi^a(\mathbf{x}) d\Gamma - \sum_{a=1}^n \hat{\theta}^a(s) \int_{\Omega_s^b} \rho(\mathbf{x}) c(\mathbf{x}) s \phi^a(\mathbf{x}) d\Omega =$$

$$= - \int_{\Gamma_3^b} h(\mathbf{x}) \frac{1}{s} \theta_{e0} d\Gamma - \int_{\Omega_s^b} \bar{F}(\mathbf{x}, s) d\Omega . \tag{28}$$

Similarly, for axisymmetric problems, the local boundary integral equation (11) for the source point \mathbf{x}^c located inside Ω or on Γ_3 yields the following set of equations:

$$\begin{aligned} & \sum_{a=1}^n \hat{\theta}^a(s) \int_{\partial\Omega_s^c} k_{\alpha\beta}(\mathbf{x}) n_\alpha(\mathbf{x}) \phi_{,\beta}^a(\mathbf{x}) d\Gamma - \sum_{a=1}^n \hat{\theta}^a(s) \int_{\Omega_s^c} \rho(\mathbf{x}) c(\mathbf{x}) s \phi^a(\mathbf{x}) d\Omega + \\ & + \sum_{a=1}^n \hat{\theta}^a(s) \int_{\Omega_s^c} \left[\frac{k_{rz}(\mathbf{x})}{r} \phi_{,z}^a(\mathbf{x}) + \frac{k_{rr}(\mathbf{x})}{r} \phi_{,r}^a(\mathbf{x}) \right] d\Omega = - \int_{\Omega_s^c} \bar{F}(\mathbf{x}, s) d\Omega. \end{aligned} \tag{29}$$

For the source point \mathbf{x}^b located on the global boundary Γ , the boundary, $\partial\Omega_s^b$, of the sub-domain is created by L_s^b and Γ_{sq}^b (part of the global boundary with prescribed heat flux) according to Fig.1. The local integral equation has in this case the following form:

$$\begin{aligned} & \sum_{a=1}^n \hat{\theta}^a(s) \int_{L_s^b} k_{\alpha\beta}(\mathbf{x}) n_\alpha(\mathbf{x}) \phi_{,\beta}^a(\mathbf{x}) d\Gamma - \sum_{a=1}^n \hat{\theta}^a(s) \int_{\Omega_s^b} \rho(\mathbf{x}) c(\mathbf{x}) s \phi^a(\mathbf{x}) d\Omega + \\ & + \sum_{a=1}^n \hat{\theta}^a(s) \int_{\Omega_s^b} \left[\frac{k_{rz}(\mathbf{x})}{r} \phi_{,z}^a(\mathbf{x}) + \frac{k_{rr}(\mathbf{x})}{r} \phi_{,r}^a(\mathbf{x}) \right] d\Omega = - \int_{\Gamma_{sq}^b} \tilde{q}(\mathbf{x}, s) d\Gamma - \int_{\Omega_s^b} \bar{F}(\mathbf{x}, s) d\Omega. \end{aligned} \tag{30}$$

The local integral equations at nodes on the part of the global boundary with essential boundary conditions $\Gamma_{s\theta}^b$ are replaced by equation (26) given by the collocation of the interpolation approximation (18).

The time-dependent fields can be obtained from by an inverse transformation of the Laplace transformed values. Several numerical inversion schemes are available for this purpose. It is also well known that for large time intervals, the numerical inversion of the Laplace transform is unstable. However, the instability due to Laplace inversion is generally lower than inverting the solution matrix resulting from undetermined boundary conditions on some part of the boundary in inverse problems. In other words, small truncation errors can be greatly magnified in the inversion process which leads to poor numerical results. For shorter time instants, the numerical results after the Laplace inversion are reliable [Davies and Martin (1979)]. Of interest here are only relatively short time instants; the sophisticated

Stehfest's algorithm [Stehfest (1970)] for the numerical inversion is used. If $\bar{f}(s)$ is the Laplace transform of $f(t)$, an approximate value f_a of $f(t)$ for a specific time t is given by

$$f_a(t) = \frac{\ln 2}{t} \sum_{i=1}^N v_i \bar{f}\left(\frac{\ln 2}{t} i\right), \quad (31)$$

where

$$v_i = (-1)^{N/2+i} \sum_{k=\lceil(i+1)/2\rceil}^{\min(i, N/2)} \frac{k^{N/2}(2k)!}{(N/2-k)!k!(k-1)!(i-k)!(2k-i)!}. \quad (32)$$

In numerical analyses, $N = 10$ is used for double precision arithmetic [Sladek et al. (2003a,b)]. This means that for each time t , N boundary value problems for the corresponding Laplace parameters, $s = i \ln 2/t$, with $i = 1, 2, \dots, N$, need to be solved. If M denotes the number of the time instants in which $f(t)$ is to be found, the number of the Laplace transform solutions $\bar{f}(s_j)$ is then $M \times N$. It is perhaps worth noting that most of the alternative methods for the numerical inversion of the Laplace transformation [Jin and Marin (2007)] require the use of complex valued Laplace transform parameter. As a result, the application of complex arithmetic may lead to additional storage requirement and an increase in computational effort.

Inverse and direct boundary value problems are described by the same governing equation. Only the boundary conditions are different, giving rise to the ill-posed nature of the inverse problem. The numerical method for the analysis can be the same in both types of problems. The basic issue when dealing with the inverse problem is the reliability of the solutions from the final system of algebraic equations obtained after application the numerical approximation procedures such as the MLPG method here. Generally, for the Laplace transform integral formulations, the system of algebraic equations can be rewritten into a matrix form with unknown quantities on the left hand side and prescribed quantities are on the right hand side:

$$\mathbf{KX} = \mathbf{F}. \quad (33)$$

The matrix \mathbf{K} in equation (33) is a square matrix with size $(N \times N)$, where N is the total number of nodes. Their terms are determined by equation (28) and equation (29) for 2-D and axisymmetric problems, respectively. It is ill-conditioned due to the ill-posed nature of the IHCP. This means that numerical results are sensitive to the "noise" on the right hand side \mathbf{F} and the number of nodes used in meshless approximation. Regularization methods [Divo et al. (2005)] are among the most

popular and successful methods for solving accurately and in a stable manner, ill-conditioned matrix equations. The truncated singular value decomposition (TSVD) is one such technique and it is employed here to solve the matrix equation. The singular value decomposition (SVD) of matrix $\mathbf{K} \in \mathbf{R}^{N \times N}$ is given by [Hansen (1998)]

$$\mathbf{K} = \mathbf{W}\mathbf{\Sigma}\mathbf{V}' = \sum_{i=1}^N w_i \sigma_i v_i' \tag{34}$$

where $\mathbf{W} = (w_1, w_2, \dots, w_N)$ and $\mathbf{V} = (v_1, v_2, \dots, v_N)$ are ortho-normal matrices satisfying $\mathbf{W}'\mathbf{W} = \mathbf{V}'\mathbf{V} = \mathbf{I}_N$. Here, the superscript ' represents the transpose of the matrix. It is known that $\mathbf{\Sigma} = \text{diag}(\sigma_1, \sigma_2, \dots, \sigma_N)$ has non-negative diagonal elements satisfying

$$\sigma_1 \geq \dots \sigma_N \geq 0.$$

The values σ_i are called the singular values of \mathbf{K} and the vectors w_i and v_i are called the left and right vectors of \mathbf{K} , respectively. The solution \mathbf{X} to the matrix equation (33) can be written as a linear combination of the right singular vectors, namely

$$\mathbf{X} = \sum_{i=1}^N \frac{w_i' \mathbf{F}}{\sigma_i} v_i. \tag{35}$$

For an ill-conditioned matrix equation, there are many small singular values clustering around zero. The solution obtained by standard methods may be dominated by the contribution of these small singular values and hence it becomes unbounded and oscillatory [Golub and Van Loan (1996)]. One simple remedy is to truncate the above summation, i.e. by considering an approximate solution \mathbf{X}^* , given by

$$\mathbf{X}^* = \sum_{i=1}^{N^*} \frac{w_i' \mathbf{F}}{\sigma_i} v_i, \tag{36}$$

where $N^* \leq N$ is the regularization parameter which determines when one starts to leave out small singular values. This method is known as the TSVD [Hansen (1998)]. The performance of regularization methods depends on a suitable choice of this parameter. To this end, the L-curve criterion [Lesnic et al. (1998), Jin and Marin (2007)] is frequently used in the TSVD. Then, the minimum-norm least-squares solution to the problem may be written as

$$\min \|\mathbf{X}\|_2 \text{ subject to } \|\mathbf{K}_{N^*} \mathbf{X} - \mathbf{F}\|_2 < \varepsilon,$$

where ε is a measure of the perturbations in the system matrix \mathbf{K} . The value N^* is determined by the value of ε .

5 Numerical examples

5.1 Moving fluid around a finite strip

A finite strip with homogeneous material properties and initial temperature $\theta_{in} = 20^{\circ}C$ is subjected to a moving fluid with temperature $\theta_e(t) = 100H(t - 0)$ all over the surface (Fig. 3), where $H(t - 0)$ the Heaviside unit step function. The size of the strip is $2a \times 2b$ with $a = 20$ mm and $b = 70$ mm. In the direct problem, the heat transfer coefficients at $x_1 = b$ and $x_2 = a$ are $h_1 = 1071.43 W/m^2K$ and $h_2 = 500 W/m^2K$, respectively. Taking advantage of symmetry, only a quarter of the strip is analysed. The remaining parts of the boundary are therefore prescribed zero heat flux. The following material data are considered: thermal conductivity $k = 50 W/mK$, $\rho c = 3768000 J/m^3K$. These geometry and material parameters are the same as those used by Duda and Taler (2000), for the purpose of comparison. The analytical solution to the problem is given in [Duda and Taler (2000)]:

$$\theta(x_1, x_2, t) = \sum_{i=1}^{\infty} \frac{2 \sin \beta_i \cos(\beta_i x_1 / b) \exp(-\beta_i^2 \alpha t / b^2)}{\beta_i + \sin \beta_i \cos \beta_i} \cdot \sum_{i=1}^{\infty} \frac{2 \sin \gamma_i \cos(\gamma_i x_2 / a) \exp(-\gamma_i^2 \alpha t / a^2)}{\gamma_i + \sin \gamma_i \cos \gamma_i} (\theta_{in} - \theta_{e0}) + \theta_{e0}, \quad (37)$$

where $\alpha = k/\rho c$ and the eigenvalues β_i and γ_i are the roots of the transcendental equations

$$\frac{\beta \sin \beta}{\cos \beta} - \frac{h_1 b}{k} = 0 \text{ and } \frac{\gamma \sin \gamma}{\cos \gamma} - \frac{h_2 a}{k} = 0.$$

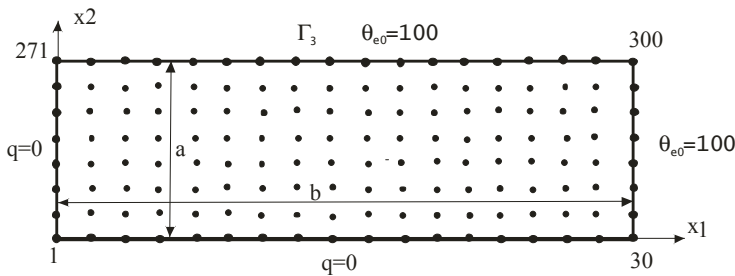


Figure 3: Boundary conditions for a finite strip

The thermal field on the finite strip is approximated by using 300 (30x10) equally-spaced nodes. The local circular sub-domains each has radius $r_{loc} = 0.0018$. The numerical results for the temporal variation of temperature at various points are shown in Fig. 4. It can be seen that there is very good agreement between the

results using the present formulation and the analytical results at the mid-point of the upper side of the strip.

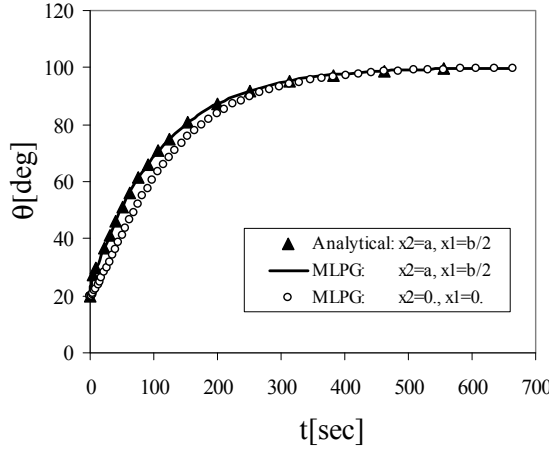


Figure 4: Direct solution: temperature distribution in a homogeneous isotropic strip at upper and bottom side

As a measure of the numerical errors, the Sobolev-norm is calculated. The relative error of the temperature in the time interval $[0, t_{max}]$ is defined as

$$E_r = \frac{\|\theta^{num} - \theta^{exact}\|}{\|\theta^{exact}\|}, \tag{38}$$

where $t_{max} = 660$ sec and

$$\|\theta\| = \left(\int_0^{t_{max}} \theta^2 d\tau \right)^{1/2}.$$

The relative errors of the temperature, E_r , at both points from Fig. 4 are less than 0.5%. For the total number of 121 (11x11) nodes, the relative error $E_r = 0.68\%$ has been obtained.

The solution to the inverse problem is investigated next. The heat transfer coefficient on the upper side is, say, unknown. Both the temperature and heat flux are unknown on the upper surface, $x_2 = a$. The temperature distribution at $x_2 = 0$ is taken from the previous analysis of the direct problem. Since the heat flux vanishes at the bottom side of the strip, the boundary conditions are over-specified on this part of the boundary, with both the temperature and heat flux being prescribed. A

requirement to obtain a unique solution [Isakov (1999)] is thus satisfied. No other internal node with prescribed temperature is considered for the inverse problem.

The Gaussian elimination method and the TSVD are both used to solve the system of algebraic equations (33) for comparison. The Gaussian elimination method was unsuccessful in yielding sensible results; the numerical outcome was highly inaccurate, $E_r = 0.35$. The relative error E_r for the TSVD is 0.0081 if no “noise” is considered for the prescribed temperature at the bottom surface. The choice $\varepsilon = 0.5 \cdot 10^{-2}$ yields $N^* = 245$. Numerical results for the temperatures are presented in Figs. 5; those for the heat flux are shown in Fig. 6. The numerical results for the heat flux obtained by the present MLPG method and analytical ones are in excellent agreement.

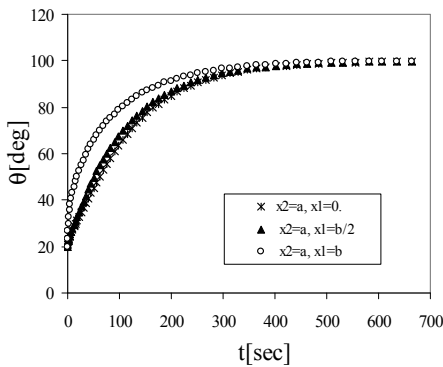


Figure 5: Results for inverse problem: time evolution of temperature at three points on the upper side of a homogeneous isotropic strip

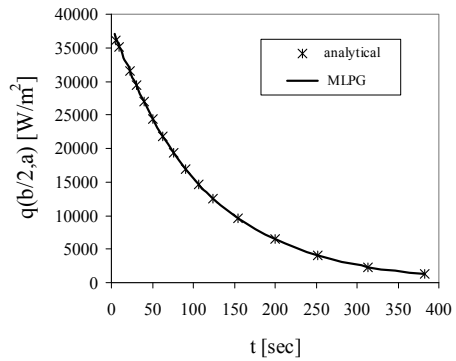


Figure 6: Time evolution of the heat fluxes at the mid of upper side of a homogeneous isotropic strip

In real inverse problems, the prescribed boundary data are measured and they are invariably contaminated by measurement errors. It is therefore of interest to investigate the stability of the computational method with “noisy” measurements. The absolute error between the noisy measurement and exact data is assumed to be bounded, i.e. $|\tilde{\theta}_i^n - \tilde{\theta}_i| \leq \delta$ for all measurement points and at all measured times. The normal Gaussian random variable function from MATLAB is considered in the numerical analyses.

Figure 7 shows the L-curve for the matrix equation (33) as log-log plot for the solution norm $\|\mathbf{x}\|$ against the residual norm $\|\mathbf{K}\mathbf{x} - \mathbf{F}\|$ for various levels of truncation in the SVD which are denoted here by dots. It can be seen that there is a steep branch of the curve for small residual norm values. The steep part of the curve

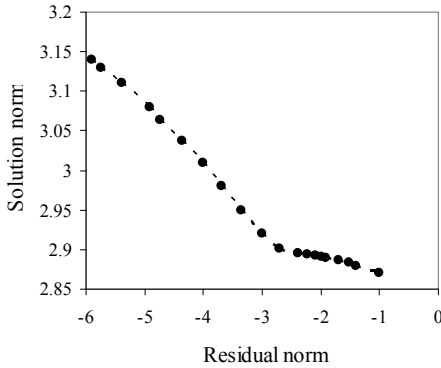


Figure 7: The L-curve for the matrix equation with 1% noise added into the data

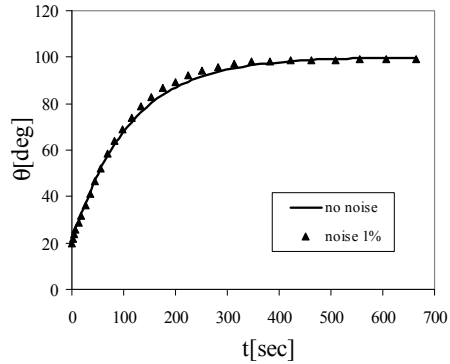


Figure 8: Influence of noisy data on temperature variation at mid-point on the upper side of a homogeneous isotropic strip

is broken at the level of truncation $N^* = 205$. This value is considered in TSVD for the solution of the matrix equation (33) with noisy input data. Next, a numerical experiment is given. In similar numerical experiments presented in literature [Lesnic et al. (1996, 1998), Lesnic and Elliot (1999), Jin B, Marin (2007)] the measurement error is considered in interval 1-2% of the nominal prescribed value. The time variation of temperature at the mid-point of the upper boundary ($x_2 = a$, $x_1 = b/2$) for noisy data with $\delta = 1\%$ is presented in Fig.8. The difference between the temperatures corresponding to noisy and noise-free data is only little bit higher than the error of the input data.

If the temperature distribution and the heat flux are computed in the inverse problem, the heat transfer coefficient is computed easily from the third equation of equation (2). Numerical results are presented in Fig. 9. A uniform and time independent value of the heat transfer coefficient has been considered in the direct problem to obtain the input data for the inverse problem. Therefore, the results presented in Fig. 9 are also a test of accuracy of the MLPG method employed. Good accuracy over the whole time interval is observed; the maximum relative error of the heat transfer coefficient is 3.4% for noisy input data.

Next, functionally graded material properties of the strip are considered whereby the thermal conductivity tensor is taken to vary linearly with the x_2 -coordinate in an orthotropic strip:

$$k_{11} = 50 \left(1 - 0.8 \frac{x_2}{a} \right), \quad k_{22} = 100 \left(1 - 0.8 \frac{x_2}{a} \right).$$

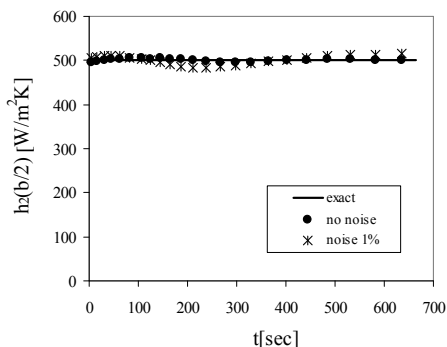


Figure 9: Numerically obtained heat transfer coefficients on boundary of homogeneous strip

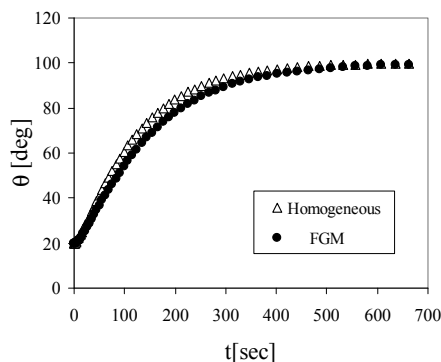


Figure 10: Direct problem: Time variation of temperatures at two points on the bottom side of the FGM orthotropic strip

In such a case the thermal conductivity on the upper side of the strip $x_2 = a$ is 5 times lower than on the bottom side. The following orthotropic material properties for the thermal conductivity are considered, $k_{22} = 2k_{11} = 100 W/mK$.

The time variation of temperature at the center of the symmetric strip ($x_2 = 0, x_1 = 0$) is presented in Fig. 10 for the direct problem. In the FGM strip, the temperature is slightly lower than in a homogeneous one. The corresponding numerical results for the inverse problem are shown in Fig. 11. The influence of noisy input data is evidently similar for the orthotropic FGM and isotropic homogeneous strips.

The numerical results for the heat flux on the upper surface of the strip are shown in Fig. 12. Results were obtained from the analyses without noisy input data. From the heat flux and temperature distributions, the heat transfer coefficient can be easily calculated.

5.2 Hollow cylinder

In the next example, an infinitely long, thick-walled hollow cylinder with inner and outer radii $a = 0.4m$ and $b = 0.5m$, respectively, is considered (Fig. 13). Since the boundary conditions along the length of the cylinder are assumed to be uniform, only a finite part of its axial section, with length $L = 0.1m$, is analyzed numerically. The external surface of the hollow cylinder is thermally insulated. The hollow cylinder with homogeneous material properties and initial temperature $\theta_{in} = 20^0C$ is subjected to a moving fluid with temperature $\theta_e(t) = 100H(t - 0)$ on the inner radius. In the direct problem, the following values were considered for the various

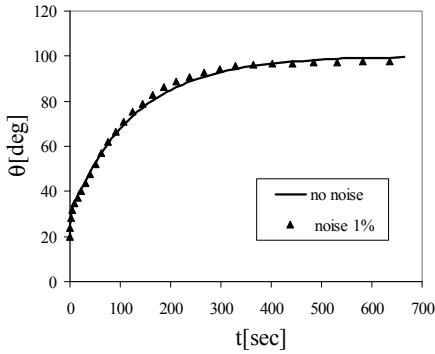


Figure 11: Results for inverse problem: temperatures at the mid-point on upper boundary of the FGM orthotropic strip

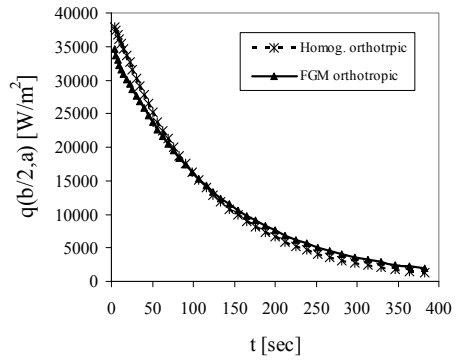


Figure 12: Heat fluxes at the mid-point of upper side of the homogeneous and FGM orthotropic strip

parameters: heat transfer coefficient $h = 500 \text{ W/m}^2\text{K}$, the thermal conductivity $k = 50 \text{ W/mK}$ and $\rho c = 3768000 \text{ J/m}^3\text{K}$.

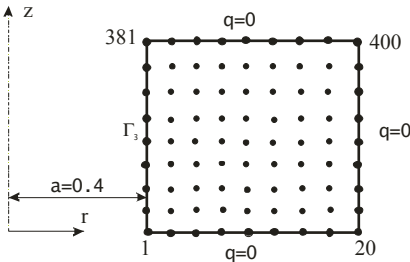


Figure 13: Analyzed domain with nodes and boundary conditions for a hollow cylinder

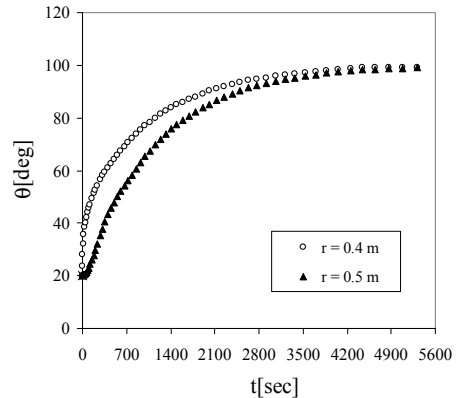


Figure 14: Temporal variations of temperatures at two different radii of a homogeneous isotropic hollow cylinder

A similar direct boundary value problem with an ideal heat transfer coefficient (prescribed temperature on the inner surface) is solved in [Sladek et al. (2007)]. In the present analysis, the thermal field on the analyzed domain is approximated by using 400 (20x20) uniformly distributed nodes. As in the previous example, the direct problem is solved in the first step. The temporal variations of temperatures at

the inner and outer radii as obtained from the MLPG method are presented in Fig. 17.

In the inverse problem, a finite hollow cylinder is considered with vanishing heat fluxes at both the ends of the cylinder. Both the Dirichlet and Neumann boundary conditions are prescribed on the external surface and no boundary conditions are prescribed at the inner radius. The values of temperature at the external radius are obtained from the solution of the direct problem.

Again the noisy input data of temperature on the external surface with $\delta = 1\%$ are used. The TSVD is applied to solve the matrix equation (33). The truncated number of equations $N^* = 231$ is obtained from the L-curve.

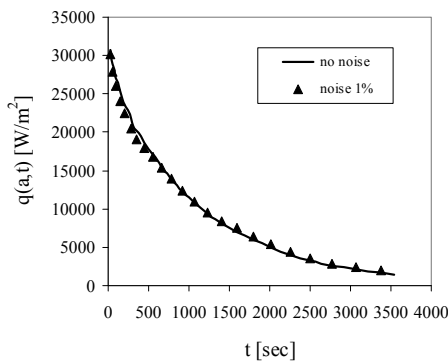


Figure 15: Temporal variations of the heat fluxes on the inner radius of the hollow cylinder

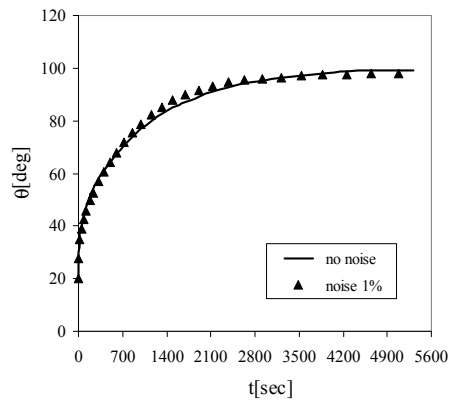


Figure 16: Temporal variation of the temperatures on the inner surface of the hollow cylinder

Solving the inverse problem, the numerical results obtained for the heat flux on the inner radius are shown in Fig. 15 for both noisy and noise-free input data. If results for noise-free input data are considered as accurate, then the relative errors of the heat flux for noisy input data are in some instants almost 15%. The time evolution of the temperature at the inner surface is presented in Fig. 16. The maximum relative error of the temperature with noisy input data to those obtained without noise is 6.5%. It is almost two times lower than for the heat flux. If both the heat flux and temperature are computed at the inner radius of the hollow cylinder, the heat transfer coefficient can again be obtained easily from eq. (2).

6 Conclusions

In this paper, a universal approach for solving transient heat conduction inverse problems in 2-D and axisymmetric bodies, and which can be employed for the determination of unspecified heat transfer coefficients has been presented. It is based on the local boundary integral equation method with the MLS approximation for spatial variations of physical fields, together with using the Laplace transform technique to remove the time variable from the governing equation. On the external surface of the body which is in contact with the surrounding fluid medium, no temperature and heat flux are prescribed (under-determined boundary conditions); on the remaining part of the boundary, over-specified boundary conditions are assumed. In the numerical test examples presented, the complete boundary data on part of the boundary are obtained from the solution of the direct boundary value problem. The material properties of bodies can be continuously varying with respect to the Cartesian coordinates. Both isotropic and orthotropic properties are considered in the direct analyses. The chosen material coefficients are then compared with those obtained from solution of inverse problems. The boundary-domain formulation can be easily implemented on simple circular sub-domains to which the local integral equations are related. In contrast to the conventional boundary integral equation methods, all integrands in the present formulation are regular due to the choice of a unit-step function as the test function. No special integration techniques are therefore required to evaluate the integrals. That the standard Gaussian elimination method for the resulting equation set from the inverse problem produces unstable results has also been shown in the present work. Stable results are obtained using truncated singular value decomposition (TSVD) applied to solve the ill-conditioned matrix equation with regularization parameter given by the L-curve method. The numerical results indicate that the present method is accurate and stable with respect to the perturbations in the input data. In future it would be interesting to compare the present results with ones obtained by promising methods [Liu and Atluri (2009a,b,c)] published recently.

Acknowledgement: The authors acknowledge the support by the Slovak Science and Technology Assistance Agency registered under number APVV-0427-07, the Slovak Grant Agency VEGA-2/0039/09. The work was also partially supported by the Research Grant Council of the Hong Kong Special Administrative Region, China (Project No. CityU 7001995) and the EPSRC research grant (U.K.) DENA1 D3R.

References

- Atluri, S.N.** (2004): *The Meshless Method, (MLPG) For Domain & BIE Discretizations*, Tech Science Press.
- Atluri, S.N.; Zhu, T.** (1998): A New Meshless Local Petrov-Galerkin (MLPG) Approach in Computational Mechanics. *Computational Mechanics*, 22: 117-127.
- Atluri, S.N.; Sladek, J.; Sladek, V.; Zhu, T.** (2000): The local boundary integral equation (LBIE) and its meshless implementation for linear elasticity. *Comput. Mech.*, 25: 180-198.
- Atluri, S.N.; Han, Z.D.; Shen, S.P.** (2003): Meshless local Petrov-Galerkin (MLPG) approaches for solving the weakly-singular traction & displacement boundary integral equations. *CMES: Computer Modeling in Engineering & Sciences*, 4: 507-516.
- Atluri, S.N.; Shen, S.P.** (2002): The meshless local Petrov-Galerkin (MLPG) method: A simple & less costly alternative to the finite element and boundary element methods. *CMES: Computer Modeling in Engineering & Sciences*, 3: 11-51.
- Beck J.V., Blackwell B., Clair Ch.R.** (1985): *Inverse Heat Conduction, Ill-posed Problems*. Wiley-Interscience Publication, New York.
- Belytschko, T.; Krogauz, Y.; Organ, D.; Fleming, M.; Krysl, P.** (1996): Meshless methods; an overview and recent developments. *Comp. Meth. Appl. Mech. Engn.*, 139: 3-47.
- Chantasiriwan S.** (1989): Comparison of three sequential function specification algorithms for the inverse heat conduction problem. *Int. Comm. Heat Mass Transfer*, 26: 115-124.
- Chantasiriwan S.** (2000): Inverse heat conduction problem of determining time-dependent heat transfer coefficient. *Int. J. Heat Mass Transfer*, 42: 4275-4285.
- Chantasiriwan S.** (2001): An algorithm for solving multidimensional inverse heat conduction problem. *Int. Comm. Heat Mass Transfer*, 44: 3823-3832.
- Chang, C.W.; Liu, C.S.; Chang, J.R.** (2005): A group preserving scheme for inverse heat conduction problems. *CMES: Computer Modeling in Engineering & Sciences*, 10: 13-38.
- Chen W., Tanaka M.** (2002): A meshless, integration free, and boundary-only RBF technique. *Comput. Math. Appl.*, 43: 379-391.
- Chen H.T., Wu X.Y.** (2006): Estimation of heat transfer coefficient in two-dimensional inverse heat conduction problems. *Numerical Heat Transfer B*, 50: 375-394.
- Chen H.T., Chou J.C.** (2006): Investigation of natural-convection heat transfer coefficient on a vertical fin of finned-tube heat exchangers. *Int. J. Heat Mass*

Transfer, 49: 3034-3044.

Davies B., Martin B. (1979): Numerical inversion of the Laplace transform: a survey and comparison of methods. *J. Comput. Phys.*, 33: 1-32.

Divo E., Kassab A.J., Karpát J.S., Chyu M.K. (2005): Retrieval multidimensional heat transfer coefficient distributions using an inverse BEM-based regularized algorithm: numerical and experimental results. *Engn. Anal. Bound. Elem.*, 29: 150-160.

Duda P., Taler J. (2000): Numerical method for the solution of non-linear two-dimensional inverse heat conduction problem using unstructured meshes. *Int. J. Num. Meth. Engn.*, 48: 881-899.

Golberg M.A., Chen C.S. (1998): The method of fundamental solution for potential, Helmholtz and diffusion equation. In: *Boundary Integral Methods-Numerical and Mathematical Aspects*, Golberg MA (ed.), CMP, Southampton, 103-176.

Golub G.H., Van Loan V.F. (1996): *Matrix Computations*. Baltimore, The John Hopkins University Press.

Guo L., Murio D.A. (1991): A modified space-marching finite-difference algorithm for the two-dimensional inverse heat conduction problem with slab symmetry. *Inverse Problems*, 7: 247-259.

Hadamard J. (1923): *Lectures on Cauchy Problem in Linear Partial Differential Equations*. Oxford University Press, London.

Hansen P.C. (1998): Rank-deficient and Discrete Ill-posed Problems: Numerical Aspects of Linear Inversion. Philadelphia, SIAM.

Hon Y.C., Wei T. (2004): A fundamental solution method for inverse heat conduction problem, *Eng. Anal. Boundary Elements*, 28: 489-495.

Hon Y.C., Wei T. (2005): The method of fundamental solutions for solving multidimensional inverse heat conduction problems. *CMES: Computer Modeling in Engn. & Sciences*, 7: 119-132.

Hsu T.R., Sun N.S., Chen G.G., Gong Z.L. (1992): Finite element formulation for two-dimensional inverse heat conduction analysis. *ASME J. Heat Transfer*, 114: 553-557.

Isakov V. (1999): Some inverse problems for the diffusion equation. *Inverse Problems*, 15: 3-11.

Jin B., Marin L. (2007): The method of fundamental solutions for inverse source problems associated with the steady-state heat conduction. *Int. J. Num. Meth. Engn.*, 69: 1570-1589.

Jonas P., Louis A.K. (2000): Approximate inverse for a one-dimensional inverse

heat conduction problem. *Inverse Problems*, 16: 175-185.

Kansa E.J. (1990): Multiquadratic a scattered data approximation scheme with application to computational fluid dynamics II. Solutions to hyperbolic, parabolic, and elliptic partial differential equations. *Comput. Math. Appl.*, 19: 147-161.

Khalidy N.A. (1998): A general space marching algorithm for the solution of two-dimensional boundary inverse heat conduction problems. *Numerical Heat Transfer B*, 34: 339-360.

Kurpisz K., Nowak A.J. (1992): BEM approach to inverse heat conduction problems. *Eng. Anal. Boundary Elements*, 10: 291-297.

Kurpisz K., Nowak A.J. (1995): *Inverse Thermal Problems*, CMP, Southampton.

Lesnic D., Elliot L., Ingham D.B. (1996) : Application of the boundary element method to inverse heat conduction problems. *Int. J. Heat Mass Transfer*, 39: 1503-1517.

Lesnic D., Elliot L., Ingham D.B. (1998) : The boundary element solution of the Laplace and biharmonic equations subjected to noisy boundary data. *Int. J. Num. Meth. Engn.*, 43: 479-492.

Lesnic D., Elliot L. (1999): The decomposition approach to inverse heat conduction. *J. Math. Anal. Appl.*, 232: 82-98.

Li J., Hon Y.C., Chen C.S. (2002): Numerical comparisons of two meshless methods using radial basis functions, *Eng. Anal. Boundary Elements*, 26: 205-225.

Ling X., Keanini R.G., Cherukuri H.P. (2003): A non-iterative finite element method for inverse heat conduction problems. *Int. J. Num. Meth. Engn.*, 56: 1315-1334.

Ling X., Atluri S.N. (2006): Stability analysis for inverse heat conduction problems. *CMES: Computer Modelling in Engineering & Sciences*, 13: 219-228.

Liu C.S. (2006): An efficient simultaneous estimation of temperature-dependent thermophysical properties. *CMES: Computer Modelling in Engineering & Sciences*, 14: 77-90.

Liu C.S. (2008): A highly accurate MCTM for inverse Cauchy problems of Laplace equation in arbitrary plane domains. *CMES: Computer modelling in Engineering & Sciences*, 35: 91-111.

Liu C.S., Yeih W., Atluri S.N. (2009a): On solving the ill-conditioned system $Ax=b$: general purpose conditioners obtained from the boundary-collocation solution of the Laplace equation, using Trefftz expansions with multipole length scales. *CMES: Computer Modelling in Engineering & Sciences*, 44: 281-311.

Liu C.S., Atluri S.N. (2009b): A highly accurate technique for interpolations using

very high-order polynomials, and its applications to some ill-posed linear problems. *CMES: Computer Modelling in Engineering & Sciences*, 43: 253-276.

Liu C.S., Atluri S.N. (2009c): A fictitious time integration method for the numerical solution of the Fredholm integral equation and for numerical differentiation of noisy data, and its relation to the filter theory. *CMES: Computer Modelling in Engineering & Sciences*, 41: 243-261.

Martin T.J., Dulikravich G.S. (1998): Inverse determination of steady heat convection coefficient distributions. *ASME Journal of Heat Transfer*, 120: 328-334.

Mera N.S., Elliot L., Ingham D.B., Lesnic D. (2000): An iterative boundary element method for the solution of Cauchy steady state heat conduction problem. *CMES: Computer modelling in Engineering & Sciences*, 1: 101-106.

Mikhailov S.E. (2002): Localized boundary-domain integral formulations for problems with variable coefficients. *Eng. Anal. Boundary Elements*, 26: 681-690.

Osman A.M., Beck J.V. (1990): Investigation of transient heat transfer coefficients in quenching experiments. *ASME Journal of Heat Transfer*, 112: 843-848.

Reinhardt H.J. (1991): A numerical method for the solution of two-dimensional inverse heat conduction problems. *Int. J. Num. Meth. Engn.*, 32: 363-383.

Shen S.Y. (1999): A numerical study of inverse heat conduction problems. *Comput. Math. Appl.*, 38: 173-188.

Shenefelt J.R., Luck R., Taylor R.P., Berry J.T. (2002): Solution to inverse heat conduction problems employing singular value decomposition and model-reduction. *Int. J. Heat Mass Transfer*, 45: 67-74.

Sladek J., Sladek V., Zhang Ch. (2003a): Transient heat conduction analysis in functionally graded materials by the meshless local boundary integral equation method. *Comput. Material Science*, 28: 494-504.

Sladek, J.; Sladek, V.; Krivacek, J.; Zhang, Ch. (2003b): Local BIEM for transient heat conduction analysis in 3-D axisymmetric functionally graded solids. *Comput. Mech.*, 32: 169-176.

Sladek, J.; Sladek, V.; Atluri, S.N. (2004): Meshless local Petrov-Galerkin method for heat conduction problem in an anisotropic medium. *CMES: Computer Modelling in Engn. & Sciences*, 6: 309-318.

Sladek, V.; Sladek, J.; Tanaka, M.; Zhang, Ch. (2005a): Transient heat conduction in anisotropic and functionally graded media by local integral equations. *Engineering Analysis with Boundary Elements*, 29: 1047-1065.

Sladek V., Sladek J., Zhang Ch. (2005b): Local integro-differential equations with domain elements for the numerical solution of partial differential equations with variable coefficients. *J. Eng. Math.*, 51: 261-282.

Sladek J., Sladek V., Hon Y.C. (2006): Inverse heat conduction problems by meshless local Petrov-Galerkin method. *Engineering Analysis with Boundary Elements*, 30: 650-661.

Sladek, J.; Sladek, V.; Hellmich, Ch.; Eberhardsteiner, J. (2007): Heat conduction analysis of 3D axisymmetric and anisotropic FGM bodies by meshless local Petrov-Galerkin method. *Computational Mechanics*, 39: 2007, 323-333.

Sladek, J.; Sladek, V.; Tan C.L.; Atluri, S.N. (2008): Analysis of transient heat conduction in 3D anisotropic functionally graded solids by the MLPG, *CMES: Computer Modeling in Engineering & Sciences* 32: 161-174.

Stehfest H. (1970): Algorithm 368: numerical inversion of Laplace transform. *Comm. Assoc. Comput. Mach.*, 13: 47-49.